.

.

Thesis To Applied for the Grade of Master of Science in Applied Physics

Albert-Ludwigs-Universität Freiburg
Faculty of Physics

Single Shot correlation in VMI- TOF measurements on He nanodroplets at MIR femtosecond laser pulses

Presented by Cristian Enrique Medina Hernandez
Date 15. febrary 2019
Referent Prof. Dr. Marcel Mudrich and Prof. Dr. Frank Stinkermeier

Abstract

In this thesis a new data acquisition method is explained for correlate single shot VMI-TOF measurements on He droplets ionized by a MIR femtosecond laser. Until now VMI images and TOF data are always treated in a statistical way. Whit these new method we expect to have some better correlation for single explosion and relate each of the event from a individual way, having specific information that could be lost in the statistical method. The correlated data is acquired by triggering the VMI camera and the TOF oscilloscope with the laser trigger, so both acquisitions begging and end after the same laser pulse. Results for the energies.....here a resumy of the results.....

Contents

List of abbreviations

ATI	above threshold ionization
BSI	barrier suppression ionization
CCD	Charge-coupled Device
CPA	Chirp Pulse Amplification
CWL	Central wavelength
EM	Electro Mechanics
LASER	Light Amplification by Stimulated Emission of Radiation
LT	Langmuir-Taylor
MCP	Micro Channel Plate
NIR	Near Infrared
pBASEX	polar Basis Set Expansion
PID	Proportional – Integral – Derivative
TBR	Three Body Recombination
TOF	Time of flight
VMI	Velocity Map Imaging
VUV	vacuum ultra violet
XUV	Extreme ultraviolet

0.1 Introduction

Physicists have always wonder to explain and resolve dynamic processes in short scale times, so initial conditions of processes can be describe in a time evolution scale. Describe any system like this requires to acquire data in shorter windows of time, for example a film is only a consecutive sequence of photographs that recreate a large time laps in a smaller time scale pics. For atomic physics, we are talking about a micro-cosmos that varies from microseconds, i.e several bodies dynamics, to attoseconds for atoms,where time scales can go down to 10^{-9} s, requiring to create measurement methods capable to record in shorter time, while the experiment have to be done in a controllable way to ensures its reproductivility, as any scientific method.

The time window of dynamics of a sytem is related to quantum dynamics, in a simple view also to its size. For dynamics happening in a molecule or a many body system interaction, the time window can oscillate between microseconds to fentoseconds, although for millielectronvolt-scale (meV) energy spacing of vibrational energy levels implies that molecular vibrations occur on a time scale of tens to hundreds of femtoseconds. The motion of individual electrons in semiconductor nanostructures, molecular orbitals, and the inner shells of atoms occurs on progressively shorter intervals of time ranging from tens of femtoseconds to less than an attosecond. Motion within nuclei is predicted to unfold even faster, typically on a zeptosecond time scale.

To achive this higth resolution in space and time physicist have challenged to create systems with a well controlled spatial and temporal gradient. Fortunately nowadays, laser pulses can research up to extreme non-linear optical processes, producing single aisolated pulses of ultra violet(UV) waves as short as 67 as [63]. Such fast pulses open up the possibility of time resolved measurements fort short processes like electron dynamics. However, to do this, experimental schemes must be devised that allow these new light sources to be used to perform measurements on the microcosmos. In particular, in the last few years, many studies at atom- and molecule-clusters had been published, From mid-infre red (NIR) interaction to UV or XUV pulses, that not just lead to a broad spectra to study but also to a large range of possible applications such as the generation of energetic electrons and ions in the keV-regime [16], as well as intensive XUV and attosecond pulses [52]. Laser pulses with peak intensitiesof up to 10^{21} W/cm^2 are available nowadays [42] commercially so the difficulty and expensive of the experiments source also are easy.

But this is never enough, Lasers is just one huge step in order to control and ignite atomic processes in controlled standard. Other step needed is how to acquire the

information we want. For this purpose several techniques are available depending the nature of the process. For this particular work we are interested in two techniques, Velocity map image (VMI) and Time of flight (TOF). Since its invention, this techniques has become two of the most commune and important measurement techniques in high energies physics. But detecting a signal is just one part of the job, the new laser advances like the generation of coherent high-intensity laser pulses with intensities up to $10^{22} W/cm^2$ allow multiphoton ionization that allows to get time resolved measurements. These advances have enabled the development of new research areas, as well as the investigation of ultrafast dynamics in highly excited matter to nanometer size.

In this thesis we focus our efforts on the ionization process by Mid Infrared (MIR) femtosecond pulses in doped He clusters. The interaction of the dopant with the Laser field result in a energy transfer to the droplet that ignite a ionization process, known as a nanoplasma. This resonant interaction of the laser field with a collective oscillation of the electrons in the plasma is driven by the laser field [16]. This process, caused predominantly by electron impact ionization, makes an avalanche-like ionization of the atoms in the cluster, leading to a heating of the plasma and, as a result, to hydrodynamic expansion and Coulomb explosion. To the analysis of this process we studied the electrons as well as the ion's resulting in the coulomb explosion. A velocity map imaging and a Time of flight technique are set up in parallel to acquire the data and reconstruct the initial energies and configuration of the plasma in study. In the First chapter we will present a brief introduction to the Droplet He generation, a short plasma interactions as a basic background of coulomb ionization in order to understand the physical meaning. In the second chapter a more detailed explanation of the set-up used is done. Showing from the creation of the He droplets process to its detection , going thorough the doping, and ignition process. For the third chapter a detailed explanation on the correlation method for the VMI-TOF measurements is done, and showing the set-up of the data acquisition and its advantages. In the fourth chapter we present the correlated data and its analysis. Finally the last chapter we present the conclusion of the experiment itself also as the data analysis and future works will needed to improve this process as well.

1 Theoretical Background

In the following chapter we will present all the theoretical background necessary for the development of this project, from the theory and creation of the He and Ne droplets to the physics theories of plasma and cluster coulomb explosion processes including its detection techniques. In order to guide the reader in an organised way, the chapters are organized in a way that follow the processes necessaries to the performance of the experiment.

1.1 Helium Nanodroplets

The combination of cryogenic matrix isolation, discovered in 1954 [61], and the now well defined properties of Helium (He), specially its superfluidity face discovered in 1937 by *Kapitza et. all* [30], have as consequence one of the most powerful and flexible tool in physics, the helium nanodroplets. Helium nanodrops have unique properties that makes it a unique source for the cluster and nanophysics experiments in the last decades. For example, they do not exhibit any optical transitions in the entire infrared, visible and ultraviolet range. They can readily pick up atoms and molecules and form different complexes of the species embedded in their interior or on their surfaces, acting as a ideal matrix for atoms, molecules and clusters isolation. [53] [58]. The size of a He cluster can go from of a few thousands up to 10^8 of atoms, and reach the ultra cold temperature regime (close to $0.37K$ [57]) [13]. Two main advantages of this cooling properties arise. First, dopants in the He nanodroplet are set to their absolute vibronic ground states, avoiding all other possible espectra and stablishing the cluster in a specific state, more important, the fast cooling helps to the formation of isomers that are difficult or impossible to generate with other methods [43]. Second, because the superfluid fase of the He nanodroplets [20], the bond between dopants and He is weak. Therefore, in contrast to spectroscopy in other matrices with higher temperatures, the optical transitions of many dopants are barely influenced by the He matrix [58]. The theory of He superfluidity will not be part of this section, this imformation is well documented in other sources, and here we are based on ref. [13] where all theory is well presented to the reader. In the

next section we will dedicate a bigger effort to explain the theoretical and technical background of the He nanodroplets creation as well as the physical and technical process to doped it.

1.1.1 He Nano droplets production

At room temperature, helium is a light inert gas. It is odorless, colorless, tasteless, and after hydrogen, the second most abundant element in the universe. [13]. It have a simple 2 atoms structure, exhibing numerous exotic phenomena whose theoretical descriptions are rather complex in many cases, i.e it characteristics of a quantum fluid. From helium exist two stable isotopes ^3He and ^4He. ^4He has two electrons, two protons and two neutrons, no nuclear spin and no total spin, pertaining to the bosonic family, while ^3He with only one neutron has a spin of $I = 1/2$ and belongs to the fermions [4].

The bosonic state $_4He$ is specially of interest, at temperature T$\leqslant$2.8K and under normal pressure has a phase transition from "normal liquid" He-I to super liquid He-II [55], in which the helium can be described by a Bose-Einstein condensation. Even the fermionic ^3He exhibits this phase transition at T$\leqslant 0.03K$ [25].

The superfluidity of $He - II$, at temperatures close to absolute zero, brings with it some unique features. The essential Properties for this include an almost disappearing viscosity in the superfluid phase, weak interaction, very efficient cooling, and the Transparency for electromagnetic radiation up to wavelengths in vacuum ultraviolets (VUV) Spectral range [13]. Helium has therefore in the complete visible spectrum no transitions from the ground state. Through the noble gas configuration, helium has a spherically symmetrical electron distribution [38], it can hardly be polarized and is the least reactive of all the elements.

1.1.1.1 Helium Droplets

The production He droplets had to overcome first one principal problem, its liquefaction. At the end of 19th century many gases were liquefied for the first time by applying pressure at room temperature. However, for He and hydrogen, this method was not successful. In 1922 Kamerlingh Onnes reached temperatures below $1K$ by reducing the vapor pressure above liquid helium to about $2*10^{-5}$ bar with a series of pumps [10]. The Joule–Thomson effect [60] is in this case the responsible for Onnes experiment to reach this low temperatures. The basic idea is that under suitable conditions a gas in expanding performs work against its internal forces. Basically the gas is expanded through a small nozzle thermally isolated from its surroundings.

Figure 1.1: ^4He Phase transition at Ultra cold temperatures. ^4He is the more common isotope of helium. It remains liquid at zero temperature if the pressure is below $2.5MPa$. The liquid has a phase transition to a superfluid phase, also known as He-II, at the temperature of $2.17K$ (at vapor pressure). Taken from [1]

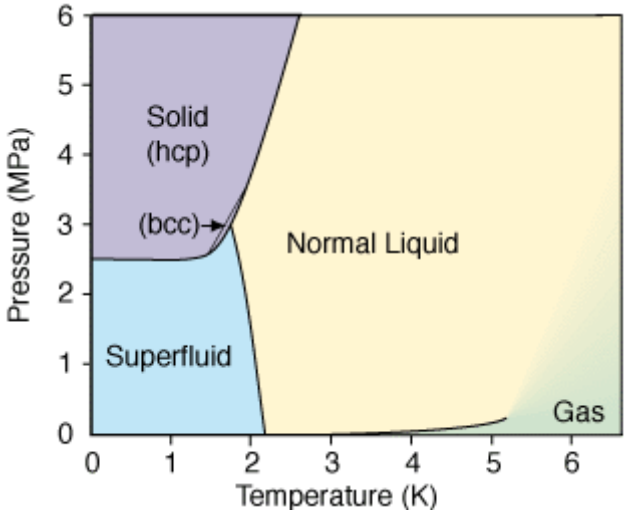

The expansion under theses conditions takes place at constant enthalpy, since the expansion nozzle performs no work. following the next relation:

$$W = H_1 - H_2 = (U_1 + p_1V_1) - (U_2 + p_2V_2) \tag{1.1}$$

where H is the entalpy before and after, $U = \frac{3}{2}Nk_bT$ for ideal gases and $pV = Nk_bT$ [13]. Under Joule–Thomson effect conditions, $W = 0$ so $H_1 = H_2$, this expansion leads to a cooling or a warming and under certain conditions, becomes supersaturated. As a result, condensation takes place and a beam of clusters is formed.

Helium nanodroplets are typically produced by a continuous or pulsed adiabatic Expansion of pre−cooled helium through a small aperture from a reservoir into a vacuum [53]. In this process a droplet jet is formed, and its characteristics (blasting speeds and size distribution) can be changes due the manipulation of the set−up. For example, $\triangle$ pressure between the reservoir and the vacuum chamber (usually in the range of a few to $10MPa$) , the nozzle temperatures(from a few K to $T \leqslant 40K$) or the nozzle size (with pinholes of diameter rounding $5 - 20\mu m$).

When the Helium expands from the nozzel, its thermal energy is transform in kinetic energy of a supersonic flow field. After the expantion into the vacuum, the gas becomes supersaturated and condensations starts to occurs, creating the beam clusters. This clusters are made of atoms or moleulces held togueter by Wannder

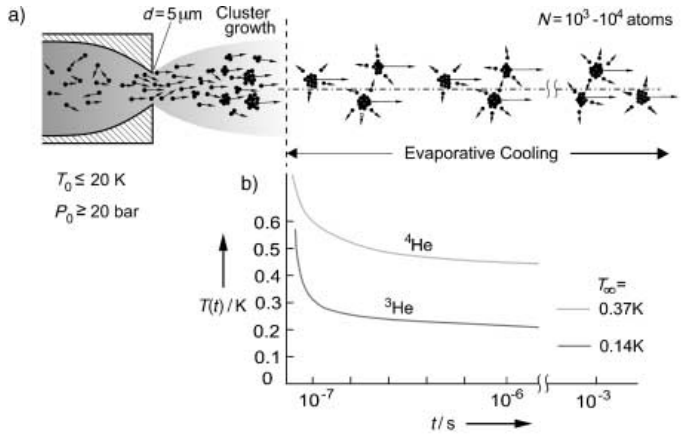

Figure 1.2: a) Schematic representation of the processes leading to the formation and subsequent cooling of helium droplets in a gas expansion. b) Calculated dependence of the droplet temperature on time for ^4He and ^3He droplets after they have left the cluster, taken from [58]

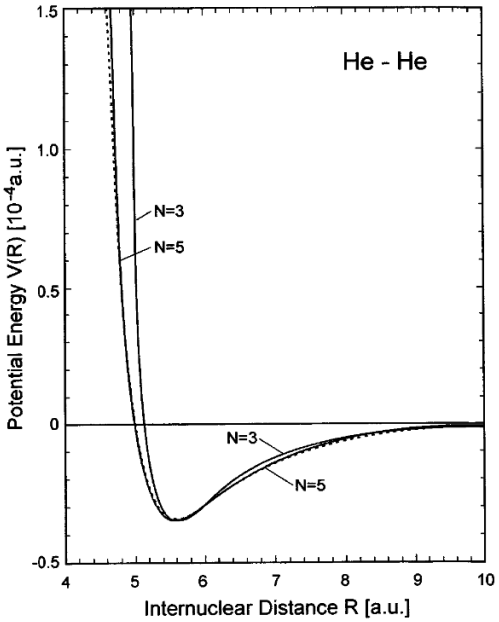

Figure 1.3: Waan der Wals potential for He-He interaction

wals fores, in this case He-He interaction, that share the same kinetic vector. This means that the two particules travel as close and parallel to each other that a bonding is possible, see fig 1.3. From the reference frame of the cluster, each of its molecules are close to cero movments, in He this enhace the conditions to be liquid and in consecience superfluidity is achive [23].

Depending on the buffer gas used, the mechanisms for cluster formation in the supersonic expansion range from condensation from the gas phase to fragmentation of a liquid phase. figure XXx show how to distinguish between these two limiting

conditions. In the case the expansion is isentropic (adiabatic and reversible), the expansion is represented by a vertical line in this diagram. Clusters formed by condensation from the gas phase occur when the expansion crosses into the two-phase region on the right-hand side of the critical point. Clusters formed by fragmentation of the liquid phase occur when the expansion crosses into the two-phase region on the left hand side of the critical point. the diagram is an example of three gases, He, Ar and H2 at diferent pressures ($p' = P/P_{critical}$,) [33]. the curves represents the regions where the supersonic expansion cam be done and the temperatures (in Fig dimensionles)that each gas should have in order to achive clustering and cooling. [33]

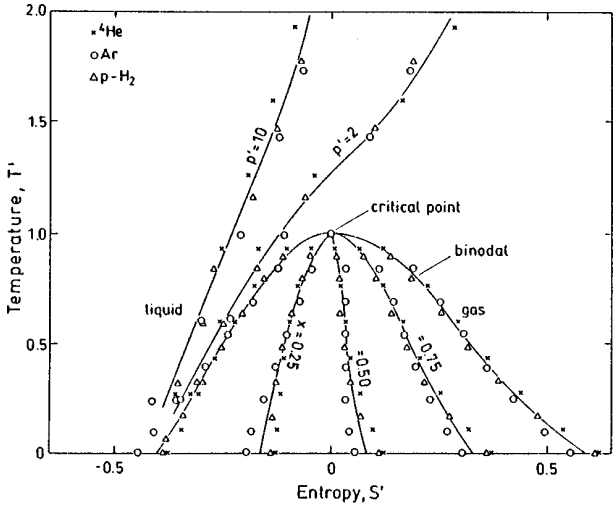

Figure 1.4: Dimensionless phase diagram for He, H2 and Ar. where T is dimensionless $T' = (T - T_{tp})/(T_{cr} - T_{tp})$, same as entropy $S' = (S - S_{cr})/\Delta Stp$ and $x = fraction$ of the fluid in the gaseous phase, where the subscripts cr and tp refer to the critical point and the triple point, and ΔS is the entropy change for vaporization. The curves are drawn as guides to the eye not exact measuments, taken from [33].

There is no mathematical approach of the physics behind this cooling expansion but usually, Raleigh scattering measurements in combination with an empirical scaling law [23] are used to estimate the mean cluster size giving a certain degree of control over the cluster size distribution by adjusting the nozzle width and the source pressure. The droplet size distribution during supersonic expansion in the follows a log-normal distribution of the form [26].

$$p(N) = \frac{1}{\sqrt{2\pi}N\sigma} \exp\left[-\frac{(ln(N/N_0)^2}{2\sigma^2}\right] \tag{1.2}$$

Where N is the number of atom in the cluster, σ is the distribution width and N_0

is the most likely numbers of atoms. Following it give a mean value.

$$\bar{N} = \exp\left(\mu + \frac{\sigma^2}{2}\right) \tag{1.3}$$

With a half width maxima of [26]

$$\sigma N_{\frac{1}{2}} = \exp\left(\mu - \sigma^2 + \sigma\sqrt{2ln(2)}\right) - \exp\left(\mu - \sigma^2 - \sigma\sqrt{2ln(2)}\right) \tag{1.4}$$

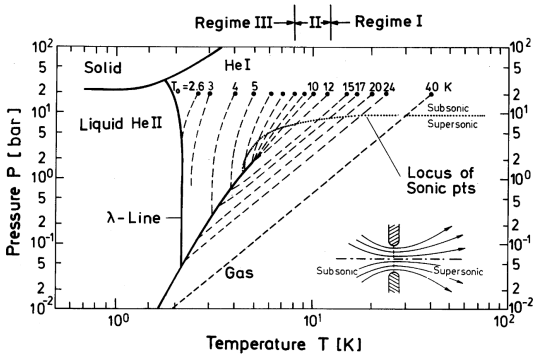

Figure 1.5: Expansion regimes. Pressure-Temperatur phase diagram for ^4He for Nozzle beam expansions starting from a stagnation of 20 bar and a temperatures. As dicusse, quialitatively different behaivors are shown for the regime I - II and II where starting in the gas phase, near the phase trnasition respectivelly. taken from [7].

As show in Figure **??** The conditions in the He (pressure, temperature and nozzle size) in the free expansion will determine the characteristics of our final He beam. From Here three main regimes can be define.

Regime I or sub-critical expansion, begins in the gas phase and leads to droplet formation via condensation. this is the case of most expansions since the pressure are located below the critical pressure P_c. Regime II, also called as critical expansion, is basically and interminable regime that includes all trajectories which are near the critical point, leading to random expansion and difficult control of the beam due the large fluctuations in density. Regime III, the supercritical expansion, starts at low temperatures where the He stops behaving as an ideal gas, expecting flashing or cavitation breaking up the liquid drops jet. [7]

super-critical and sub-critical regimes have been studies in the last several years and are clearly identified in the resulting size distributions. Figure **??** shows that supercritical expansion forms large droplets (usually between $20-100nm$ diameter) while a sub-critical expansion is suited to generate small droplets (around $5-10nm$). A simple relation that can be done to calculate the size or number of atom in a Custer

is using.

$$r = N_{1/3} * \rho A \tag{1.5}$$

Where r is the radius of the beam, ρ is the density, in thhis case of He $\rho = 0.0022A$ [54], but this approximation is not exact due the variation Of He density at this temperatures. As expected in both regimens for creating larger helium nano droplets, higher helium pressure and lower nozzle temperature are used. For our experiment a $5\mu m$ nozzle was used at temperature oscillating between $11 - 15K$, at pressure of $30to50$ bar.

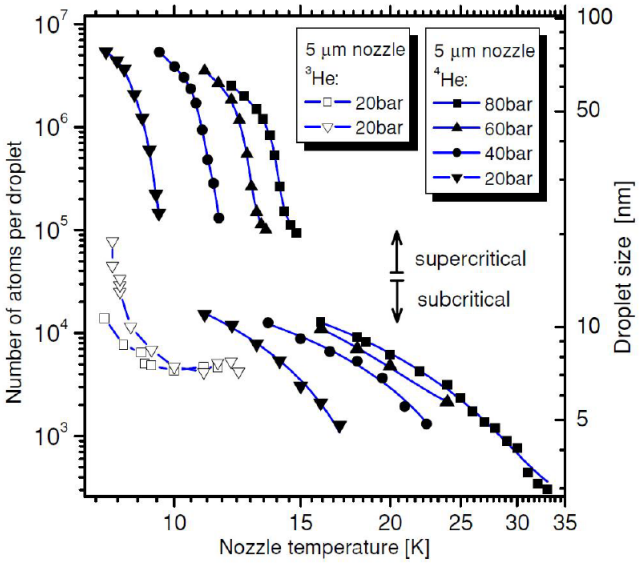

Figure 1.6: Sizes of the ^4He droplets as a function of nozzle temperature T and pressures, based on [57], using a $5\mu m$ nozzle. The sub and super critical regimes are clearly diferenciated. Taken from [?]

1.1.1.2 Composite Clusters

We can define a composite cluster or doped cluster, as a atom bulk of one material that contains one or more different atomic elements. The main interesting properties in non doped clusters are usually set as a function of its size, but for doped clusters, the interaction between the elements creates new degrees of freedom that makes more complex its behaviour. For example, the new composite will have different structural properties due the spatial distribution of the species. Hence, composite clusters exhibit a more diverse behaviour and offer more opportunities to study different characteristics of the material.

The first problem to overcome in composite cluster is how to create them. Two techniques can be used. The first one, is the co expansion of a previously mixed gas [56] or the He cluster is produced first and then crossed with an atomic beam of the doping species.

The first technique involves several technical problems, depends on possible interactions between the elements, the condensation ranges of the bulks and even in the affinity of the materials. One of the most used techniques, and the one used in this study is the one called pick-up technique [19]. The idea is simple, as well as a snowball on its way downhill collects or pick-up more snow. The He cluster, after being directional selected through a Skimmer, passes through a doping cell with a dopant gas at low densities $(10 - 2Pa)$ [53]. As a result, the gas atoms that are along the droplet cross sections will be captured by the beam and travel with it. The probability for helium droplets to collect k atoms or molecules via inelastic collisions depends on the length of the oven cell l, the cross section of the droplets σ, and the particle density inside the cell n. As l and σ remains constant, varying the density in the doping cell can regulated the abundance of k, following the Poissonian statistics.

$$P_k(l, n, \sigma) = \frac{(ln\sigma)^k}{k!} e^{(-ln\sigma)} \tag{1.6}$$

Two important properties of these relation can be infer. First the maxima of different cluster sizes are equidistant, $n_{max} = \dfrac{k}{l\sigma}$ and second, the exponential function in equation becomes nearly one for small particle densities [6].

Every pick-up process leads to an energy transfer to the droplets. As the dopant rapidly cool down to their, it means a transfer of energy to the He causing an evaporaton of helium atoms to keep the temperature unchanged. This He evaporation or "shrinkage", leads to a decrease of the cross section of the droplet and the probability to collect a further particle is reduced. The involved energy is composed of the following contributions [6].

$$E = \langle E_{kin} \rangle + E_{in} + E_{binding} + E_{cluster} \tag{1.7}$$

where

$$\langle E_{kin} \rangle \approx \frac{3}{2} k_b T + \frac{1}{2} m v^2 \tag{1.8}$$

is the kinetic energy of the droplet depending on it mass and velocity and temperature in the gas cell.

At a certain energy entry, the complete droplet evaporates if to may dopping acces

to it. With E_{kin} the average kinetic energy, E_{in} the internal. Several studies have studied the $E_{binding}$ with ^4He, given a broth number of materials to work with.. it also importat to take into acount that the binding energy include the cluste dopant binding as well as the dopant−dopant relation. [57]. Acommung energy bounding for example $Xe - He$ is arround $26.9meV$ [37], or $He - H_2O$ is about $0.1eV$ [38]. A more detailed table of all the energy bounding energy used in this study can be found in the appendix.

1.1.2 Neon Droplets

Ne is the second lightest inert gas with atomic number 10, it have 3 isotopes, the ^{20}Ne with more than 90% of abundac, followed by ^{21}Ne and ^{22}Ne, all of them can be found stable in nature [41]. As a nobel gas, it shares most of the properties already mentioned for He, excepted for its superfluidity. It have a a quite large Ionization potential for the firs electron at $Ip = 21.56eV$, what makes it quite suitable to use with strong fields lasers, as a matrix, because at low intensities it will not interact (get highly ionized) with the laser field, so Dopants can be carried in a non interactive way.

At extreme temperature, Ne is solid as shown in the graphic XXX, althougth it triple point and solidification limit allow it to be used at extream low temperatures too. Its triple point is arround $T_p = 24K$ [62] and have a rather high initial Ionization Potential.

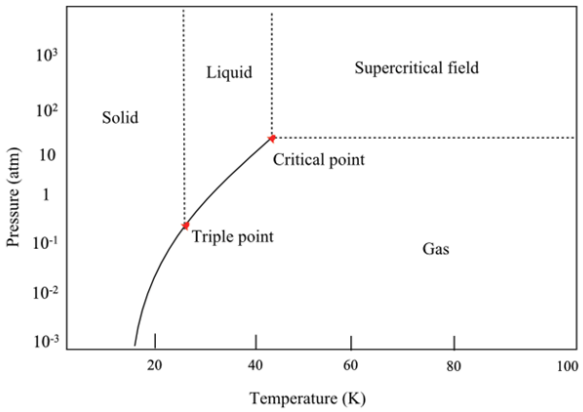

Figure 1.7: on the left. Neon phase diagram. taken from [62],on the right, $T - S$ phase diagram of Ne. The critical point is located at $T_c = 44.49K$ and a molar entropy of $S_c = 30.76J/(molK)$. The dashed lines represent regions. Taken from [8]

Ne cluster also provide an ideal medium for quemichal reactions as solvation effect and heterogenius chemestry at a miscroscopic level [19]. With a proper regulated

pick-up system teh reactants are deposited in a controlled way in the cluste and the cluster becomes a nanoreactor. in the same way, the low temperatures at the Ne the reactants will dicresse the ere degrees of freadom and act in a more basic and predictable reactions. [18].

The conditions for creating Ne clusters are quite similar to the ones explanied above, also well explained in the famus Hagena law [24], for different temperatures and nozzels. Several studies have been realized on the characterization of Ne clusters have been achieved. One example is by *R. von Pietrowski et all*, on contrary to the He clusters, on Ne is important to work at temperatures and pressures far from its solidification point. At extream low temperatures, diferences in preasure leads to a change on the size clusters, the higher the preassure in the nozzle the bigger the droplets. As example in *Pietrowski* work,, was shown that small droplets, $N = 300$, been N the number of atom in the cluster, are in a "liquid" stade but for bigger droplets solidification is present. In addition, the location of the doppant also will be affected drastricly by these sizes changes. When the droplet is on a "liquid stade" the dopants atoms are more free to move to the center and arrond the cluster, but in a more dense droplet, this dopant will tendt to stay in the surface of the same. [44].

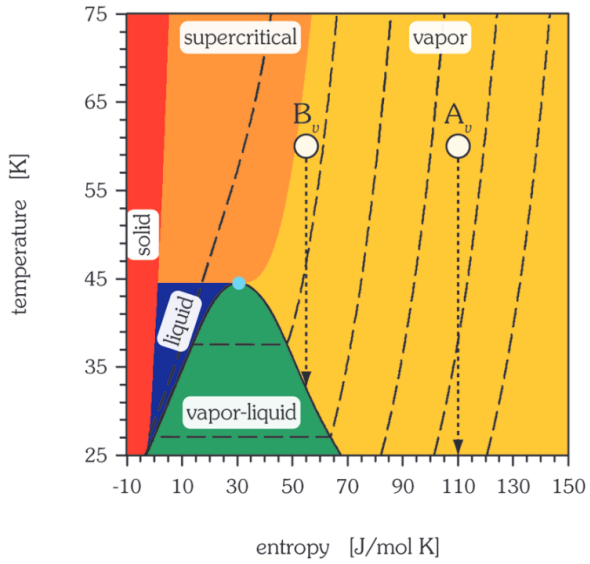

Figure 1.8: on the left. Neon phase diagram. taken from [62],on the right, T−S phase diagram of Ne. The critical point is located at $T_c = 44.49K$ and a molar entropy of $S_c = 30.76J/(molK)$. The dashed lines represent regions. Taken from [8]

Same as the T-S representation of He,Fig **??**, fig **??** shows the isentropic processes as simple vertical trajectories. One advantage in this color plot (color available on-line) is the visibility of the two-phase region where condensation may take place. The dashed lines represent isobar lines at $p = 100, 1000, 1000, 10000$, and $100000\ Pa$

from left to right respectively. SOn one hand, upersonic expansions which originate in the vapor phase at a very low source pressure, equivalent to a comparatively large stagnation entropy s_0, will not reach this region. On the other hand, for negative entropies the solid state is always reached and for low temperatures ad relative small entropy the liquid state is the predominant. In contrast, supersonic jet expansions which originate at high source pressures will arrive at the saturation curve. Thermodynamically, condensation is feasible at the gas-liquid phase boundary. Accordingly, isentropic expansions reaching the binodal line (Magenta point in the peak of the Vapor-liquid phase) might be expected to yield both uncondensed particles and condensed species such as clusters and droplets. Hence, for sufficiently high pressures it is shown from this phase diagram to expect always a gaseous beam; this is irrespective of the initial reservoir temperature.

1.2 Cluster-Intense Fields Interaction

To understanding of the interaction atoms-fields have been study broadly in physics since Einstein Photoionizasion Theory [12], that gives a base on all the quantum electrodynamics theory. The basics unders this theory is the behaivour of ligth as a electromagnetic field where the electron as a bounded charge in the atom can be afected. This quantum dynamic theory is well understood since 1957 for small atoms, with one, two or few electrons [3], but still big molecules and atoms have been challenging scientific for years. In this chapter we will give a brief introduction to the photoionization process, explaining at the same time multi-photoionization and tunnelling precesses, so we can finish with a more detailed presentation of Strong field interaction with clusters and the Keldish theory.

1.2.1 Photolonization for single atoms

The process of photoionization describes the leaving of an electron from its bound state into the continuum by interaction with electromagnetic field radiation [5]. The atomic bounded electrons while going through an electro magnetic field, in our case the laser beam, can absorb enough energy to get excited and fly away from the nucleus. A bound electron only can escape from an atom by absorbing photons its energy exceeds the binding energy of an electron [12]. When the photon energy of the laser is smaller than the ionization potential of the target, the electron can absorb two or more photos in the ionization process, this is called Multi photon ionization (MPI). Another possible process is called, tunnelling ionization, where due the quantum mechanic properties of the electrons under certain conditions absorb

enough energy enough to be on an above threshold regime and due it quantum dynamic properties it can escape from it bounds via tunnelling.

There is a variety of theoretical approaches to describe interaction of laser fields with atoms. The Hamiltonian of the system of N particles (ions and electrons) with pair-wise Coulomb interactions under the action of an external time-dependent electric field has the form:

$$H = \sum_{1 \leqslant i \leqslant N} \frac{P_i}{2m_i} + \sum_{1 \leqslant i < j \leqslant N} \frac{q_i q_j}{\mid r_i - r_j \mid} + \sum_{1 \leqslant i \leqslant N}^{n} q_i r_i \varepsilon(t) \tag{1.9}$$

where r_{i,p_i} and q_i are the coordinates, momenta and charge of the particles including the interaction between the classical electric field and $\varepsilon(t)$ where [42]

$$\varepsilon(t) = \varepsilon_0 e_z cos(\omega t + \varphi) \tag{1.10}$$

The proces that drives ionization can be divide on two regimes, a quantum electrical regime and a clasical one. [31]. Equation 1.9, use the non-relativistic approximation and neglect contributions from magnetic fields. The classical description of the laser field is a good approximation for intense enough pulses, otherwise, quantum electrodynamics description is necessary.

An electron in the initial level with enery E_i can absorb an photon with energy $\hbar\omega$ leading to final transition where $E_f - E_i = \hbar\omega$, when the enrgy of the photon is larger than the bounding energy, or the Ionization barrier the elctron is free with a the remainin kinetic energy $E_{kin} = \hbar\omega - I_{pot}$ [2]. In classical mechanics the probability of the energy transition depends directly on the cross section (σ) of the electron in it was of the field However, in quantum mechanics, the photoionization cross section is related to the its transition probability between the initial and the final state given by Fermi's golden rule

$$W_{|i\rangle \to |f\rangle} = \frac{2\pi}{\hbar\hbar} |\langle f|H|i\rangle|^2 \delta(E_i - E_f - \hbar\omega) \tag{1.11}$$

$$\sigma(\hbar\omega) = \frac{2\pi}{3} \alpha a_0^2 \hbar\omega |\langle f|r_n|i\rangle|^2 \tag{1.12}$$

When eq. 1.11 is thee transition probability of one lectron to jump from minitial state i to final state f, where H is the hamiltonian operator. Eq. 1.12 is the consequent cross sectiononsidering only the dipole part of the interaction Hamiltonian, where α is the fine structure coefficient, r_n is the position operador of the electron n [17].

Energy photon needed to ionize an atom is directly proportional to the the ener-

getic distance between the electronic states and the ionization threshold. For states closer to the ionization potential a VUV photon can be enough to free a electron but for inner electrons higher photon energies are required, varying from several tens eV to the order of several tens of keV, needing radiation sources at shorter wavelengths such as XUV to X-rays. [2]

After photoionization is done, the electronic structure of the atom needs to rearrange via, due to the vacancy left by the ejected electron. Two relaxation processes can happens during this time. An electron from the outer shell will decay and replace the freed one, therefore the energy difference of the needs to be released in form of a fluorescence photon or Auger electron. On one hand, in case of a fluorescence decay the ionic state of the target does not change, since no additional electron is release. on the other hand, the Auger decay is a non radiative relaxation process, where a second electron is released from the Coulomb potential of the ion.

In example. as shown in fig.... if an photon whit energy $\hbar\omega > E_{bin}$ ionized an electron, this will leave the atome lefting a gap. An electron in the higers level will replace the outer one, and lefting an ecxcess of energy. The outcome will be a fluerecence process with $E_{flu} = E_{in} - E_{out}$ or , the Auger $e-$, if $E_{in} - E_{out} > E_{bond}$ and this electron can also escape the atomic Coulomb potential [50].

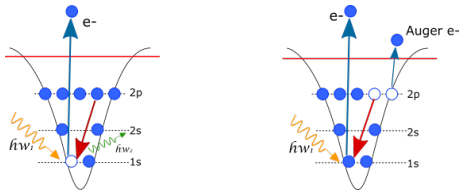

Figure 1.9: two example os the relaxation processes. On the left, A photon ionized an electron and the Electron Ein replaced, expelin a fluerecent photon in the process. on the rigth, the energie reliessed by the replacement electron is enougth to make another electron in the outer shell to also go to the continium, ASuger electron. taked form [47]

1.2.2 Multiphoton and tunelling Ionization

Ionization is also possible even when one photon energy is lower than the binding potential. Laser fields with intensities below $I \leqslant 10^{14} W/cm^2$ are not strong enougth to change the binding potencial of an atom significantly [48] and is when mUltiphoton Ionization takes place (MPI). MPI is the simultaneous absorption of several photons to overcome the ionization barrier. The way MPI occurs depends on the laser frequency and intensity. When the intensity is much lower than the characteristic atomic resonance, MPI occurs via transitions through virtual states.

Ionization by several photons at low laser intensities can be realized by the so-called resonance enhanced multiphoton ionization (REMPI) [40]. Ionization by a REMPI process takes place in two steps First, a resonant excitation by one or more photons takes place on an electron state of the atom. In the second step, this electron state is transformed into a virtual state, to an upper state until the electron is excited by spontaneous decay. So for example the total energy absorbed by an election until it gets ionizes is $n * \hbar\omega > I_{pot}$ where n is the number of photon absorbed until it actually have enough energy to overcome the potential I_{pot}

For Laser intensities $I > 10^{14} W/cm^2$, higher intensities and lower frequencies, tunneling ionization (TI) is more likely to occur. In this case, the binding potential of the atom get is strongly afected by the electric fiels of the laser. Arround the peack of the electri field the potential gets narrower, and the electron in the outer states get closer to the bidding barrier, allowing the electron to tunneling througth the confining potential into de continium [21]. TI is inherently a quantum process. The bending of the Coulomb potential becomes by the superpossition of the coulomb potential and the laser field. Therefore TI must occure when the time of the ionization is shorter than a laser oscilation cycle [5]. Based in the same principle, when the Laser fiel becomes so strong to lower the binding potencial that separates the highest electron level, then the electrons in this state become free electrons. This process is called barrier suppression ionization or BSI [35].

In the fig **??**, we present a sketch of the 3 possible ionization processes explained above. On the left we present a simple ionization process where a photon with energy $E_{phot} = \hbar\omega$ is higher than the potential barrier. In the center a MPI process is shown, n photons exite the inner-shell electron, exiting it througth virtual level until it finally have enougth energy to be free to the continium. Finally on the left a TI happens. Here the coulomb potencia barrier is afectis by the laser files bending, the outter shell electron gets closets to it nuntil it tunnels [47].

As explained the Intensity of the external fiel plays an important rol in the ionizaion process. A rather easy way to differenciate when each process needs to be taken into account is provides by the Keldysh parameter [32].

$$\gamma_k = \sqrt{\frac{I_p}{2U_p}} \tag{1.13}$$

Where γ_k is the Keldish parameter, I_p is the atoms ionization potential and U_p is the ponderomotive potential defined as

$$U_p = \frac{e^2 E_0^2}{4 m_e \omega_0^2} \propto I\lambda^2 \tag{1.14}$$

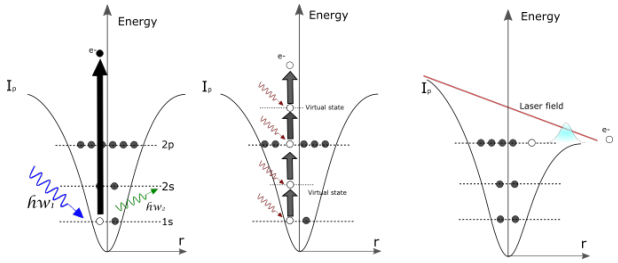

Figure 1.10: On the left is the scketch of a single photon ionization process, where a photon with energy $E_{phot} = \hbar\omega$ is higher than the potential barrier I_p. On the center the MPI process, inner-shell electron absorbs n photons, getting excited througth the electronic levels (reals or virtual) until it reach the continium. On the left the BSI Process, the coulomb potencial barrier bends by the laser fields, been lower than the outer shell electron state, the electrons can scape easilly. based on [47].

where m_e is the mass of the electron, ω_0, λ, I and E_0 are the frequency, wavelength, intensity and the peak of the electric field of the laser pulse. On one hand, when the Keldish parameter is higher, $\gamma_k \gg 1$ MPI regime is consider. On the other hand, the $\gamma_k \ll 1$ describes the TI interaction.

1.2.3 kelysh Theory

in this section we will give abief introduction to keldysh theory andn the main repectutions for our work as the ionization rates. we where based this subchapter in the work of Keldy et all, [32], and the papers review of the theory by [45] and [31]. For a deeply explanation we recomend the reader to reference this works.

The keldysh Theory, also known as the Keldysh–Faisal–Reiss theroy (KFR), is well used for the description of quantum process induced by intense laser radiation. The applications and advantages of Keldysh formulation in many-body theory among can over come from, treatment of systems away from thermal equilibrium (with or wothpout presence of external fields), solutions in supersymmetry methods of systems with quenched disorder to the calculation of the full counting statistics of a quantum observable [29].

According to the Keldysh ansatz, the transition probability amplitude between an atomic bound state and the continuum by the value of the photoelectron momentum p measured at the detector is given by: [45].

$$M_k(p) = -\frac{i}{\hbar}\int_{\text{inf}}^{+\text{inf}} \langle \Phi_p \mid V_{int}(t) \mid \Phi_0 \rangle dt \tag{1.15}$$

Where M_k denotes the Keldys transition probability, Φ_0 is the bond state wave

funtion unperturbed and Φ_p is the caonical momentum equal to p, also known as the Volkov Funtion, and V_{int} is the electron field interaction operator. If the amplitude of ionization $M_k(p)$ is known the differential probability to find the photoelectron in the elementary volume near the momentum p is givwen by the momentum distribution of the photoelectrons

$$dW(p) =\mid M(p) \mid^2 d^3p \tag{1.16}$$

givin a total probability of

$$W = \int \mid M(p) \mid^2 d^e p \tag{1.17}$$

meaning thet for enougth long pulses containing a large number of optical periods so that its electromagnetic field is close to a periodical function of time close to the initial, it is physically more appropriate to use probabilities per time unit (rates) instead of time-integrated values. .

.

.

.

.

.

.

1.2.4 Ponderomative energy

As soon as an electron is release into the continuum, it is under the influence of the external laser field. A description of the energy that it acquires during this interaction is given by the ponderomotive energy (PE).

$$U_p = \frac{e_2 E_a^2}{4m\omega^2} \tag{1.18}$$

Where m and e is the electron mass and charge, E_a and ω_0 amplitude and frequency of the electric field respectively. The formula of the ponderomotive force can be easyly derived as shown in [46] [9]. Lets consider a polarized electric field (in a.u).

$$E = \widehat{z} E_a sin(\omega_0 t) \tag{1.19}$$

considering only the $\widehat{z}$-components so we can avoid the vector sign. by classical mechanics we have.

$$p(t) = -\int_{t_0}^{t} E(t\prime)dt\prime = \frac{E_0}{\omega}(cos(\omega_0 t) - cos(\omega_0 t_0)) \tag{1.20}$$

The term at the left of the parenthesis is knows as the time varying Quiver terms, and on the one on the right, reefers to the drift motion. turning our fields in terms of vector potential we will have

$$E(t) = \frac{\delta A(t)}{\delta t} \tag{1.21}$$

$$p(\infty) = A(t_0) = -\int_{-\infty}^{t} E(t)dt = \frac{E_0}{w}cos(w_0 t_0) \tag{1.22}$$

so in the case where the pulse duration is big $t \longrightarrow \infty$ the $p + A(t) = 0$. This means that the momentum acquired by the electron will depends on the phase it is realized wt. Since the electron can be unbound in any phase of the laser pulse, will have an average kinetic energy described by

$$U_p = \frac{1}{2\pi}\int(-\frac{E}{w}cos(wt))^2 d(wt) = \frac{E_0^2}{4w_0^2} = \frac{{p_{max}}^2}{2} \tag{1.23}$$

The pondemorotive energy also gives the maximum momentum that an electron can acquire (eq. 1.22), given at the maxima . The ωt phase relation, defines what its called*the three step model* showed in figure . The first step correspond to $\omega t < \pi/2$ where the laser field is suppress, and as explained above, TI or BSI can take place. The second step, is where $\omega t > 3\pi/2$, on contrary step 1 the potential barrier is enhance, electron in the continuum that was winning kinetic energy is catched by the potential again, driven back to the atom. Finally the step 3 at phase $\omega t = n * \pi$, for $n01, 2, 3....$ At $n = 2$ it is called "recollision process" of the electron. Where the electron can be catch by the potential again, and the excess of energy cause realising another bound electrons depending on the kinetic energy necessary [34]

If we transform the eq. 1.23 to laser intensities we will have $U_p = 9,33 * 10^{-14} I[W * cm^{-2}] * \lambda^2[\mu m]$. For a MIR-pulse with intensities $\sim 10^{14}[W/cm^2]$ and $\lambda \sim 3200[nm]$ we have electron energies between one and hundred of eV.

1.2.5 Cluster Ionization

Until now, we have shown one of the most known ionization processes for single atom. But on cluster ionization, the dynamics are quite different and need a bit more detail. Clusters are combinations of atoms or molecules which, depending on their species, are held together by Van der Waals forces, ionic bonds or metallic

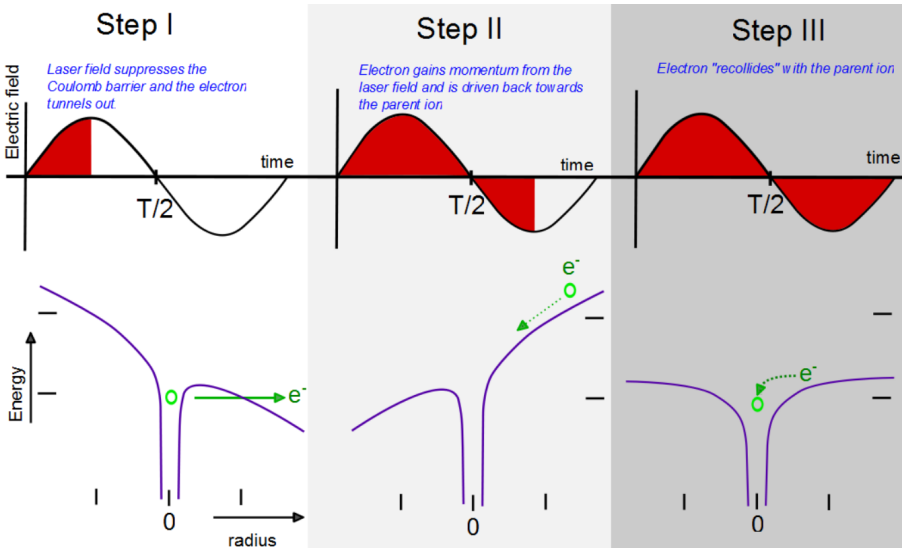

Figure 1.11: Recollision process at the three step model. Taken from [35]

bonds. In this explanations we refeer only now and on to He cluster, wich maynly are just afected by Van der Walls atraction. The investigation of clusters is of scientific interest in many studies, a clusters can be generated in a wide range of sizes (10^2 to 10^7) [53], having a radius significantly smaller than the MIR laser pulse wavelength used on them, meaning that all its atoms are equally affected by the pulse filed, in other words it penetrates all over the cluster.

The first problem that He cluster faces is auto-ionization. Been a rare gas its ionization potential is higher than much of its dopping molecles used, for example, under MIR lasers He clusters needs $I > 10^{15} W/cm^2$, so TI or BSi is not the main process at beggining of the plasma generation. Other interactions have to be explained in order to describe the process properlly. This section we will be base on *Saalaman et. all* work [49] and *Grüner et. all* [22], for this purpose we will divide the process in three phases or stages.

The first stage, called *"atomic ionization"*, the dopping atoms are ionized independently of each other by the electric field at leading edge of the laser pulse, it occurs mainly through inner ionization, especially on TI or BSI. The resulting free electrons acquire positive kinetic energy and have two option, leaving the cluster or they stay inside the cluster attracted to its positive ion core. After the first stage, the cluster nanoplasma is *ignited*, consisting of ions and quasi-free electrons, electrons taht are free to travel inside the cluster volume but still not into the continium [36].

The second stage is the *nanoplasma expantion*. During this stage the cluster is still interacting with the laser field, acquiring, by a large number of processes, energy in atoms and electrons. Ions are further created by a combined force of the laser and

other ions, the *ionization ignition* [22]. Quasi-free electrons oscillates, driven by the laser pulse and are heated to high temperatures. The heating becomes extremely efficient when the collective oscillations of quasi-free electrons become resonant with the laser pulse, Triggering a cascade reaction to more outer ionizations , and freen the remaining electrons in the cluster, this process is calles *plasma resonance* [49].

After the laser pulse is over, the last stage starts. The ions continue to expand, in consecience the radius rises as same as its cluster potential becomes smoother. In consecuence, it is easier for the highly energetic quasi-free electrons to leave the cluster, forming a coulomb explotion that destroys the cluster in a beutiful ions-electrons cascade. this proces was first describe by *Ditmire et. all* [11] combining high energetic collisions with cluster resonance absorption.

The graphic **??** shows on the left how the cluster potential is compose by the Van der Walls potential and atomic forces of the different atoms that compose the cluster. On the central images, additional to the atomic biddings, the electrical force due the ions in the cluster increase the potential, the laser pulse is still on and the quasi-free electron will gain energy wile they are in this. Finally on the right the laser field is off, the electrons have fled away and the cluster ion have repelled each other so the potential is reduced to the minimum(just atomic interactions.)

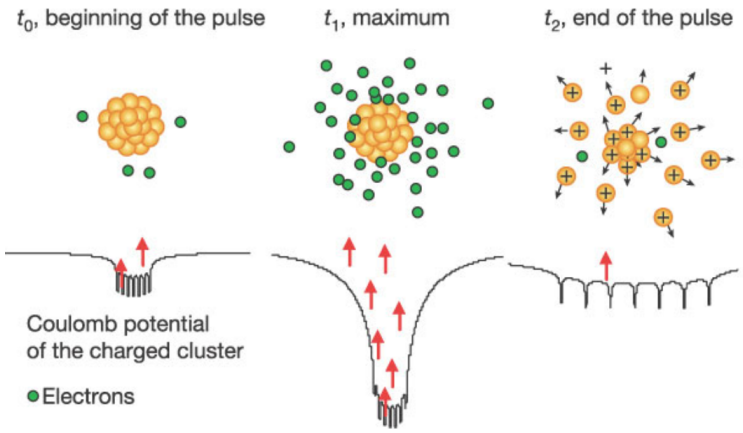

Figure 1.12: Cluster potential regimes. On the left, the atomic ionization starts the plasma formation. On the center, The quasi-free electrons auto-ionize the cluster, increasing the potential barrier and gaining energy due the laser field so a coulomb explosion can take place. On the right, The Coulomb explosion is finish, the potential is driven to it minimum and all the electrons and ions are ejected. Taken from [59]

.

1.2.5.1 Cluster expansion

Depending on the droplet size and the laser intensity, the Cluster can expand in two different ways. If the laser intensity is rather high and the droplet is small, a Coulomb explosion can occur. On contrary, if the laser is not intense enough or the droplet is too big, a nanoplasma can be generated, therefore an hydrodynamic expansion will take place. Two forces are really important during the cluster expansion. both act on the cluster during the phase two and three(during and after the laser pulse). The first, is the force associated with the free electrons with high kinetic energy. These hot electrons expand and pull the low energetic electrons and heavy ions on its pad [11]. The other force acting on the cluster is due the inner cluster charge itself. The hottest electrons in the cluster will have a mean free path large enough so they can free stream directly out of the cluster, and, if the electron's energy is large enough to overcome the space-charge buildup on the cluster, they will leave the cluster altogether. If the charge buildup is sufficiently large, the cluster will undergo a Coulomb explosion [27]. Acording to madison et all, a time scales for the laser pulse duration where the coulomb explosion can take place should be closer or lower to the femtosecond regime, depending of the element compossing the cluster. [39]. Based ont he laser power available on moder laser pulses, the same studie present that electron after a coulomb explosion can get kinetic energy up to 6KeV.

When the intensity is not enougth to make the atomic bonds to break, the electrons reamins in the cluster forming a hydrodynamic expansion as a result from a conversion of electron-thermal energy to directed kinetic energy [15]. The effects that the expansion has on the electron temperature can be calculated by equating the rate of change of radial kinetic energy from the thermal contribution with the rate of change of thermal energy within the cluster. When this condition are fullfill. the electron can present a resonance condition in the cluster, traveling in the space-charged forces formed by the plasma, winning enougth kinetic energy untill all the system collapse.

XXXX try to get the figure of ERKXXX

Althoug the two model are different in each regime. for exmaple for low kinetic energys or the begining of the pulse, the cpoulomb explosion produce less ions for low energies compared to the produced on hydrodynamic explotions. on contrary win term of hig energetic ion the coulomb explotion can crate (altho in less quantity) hotter ions than the hydrodynamis. We have to take into account that even tthe two processes are described for different laser regimes. Both porocess can happend parallel to each other, but at certain energys is clear that one or the other will be the responsable at the end for the collapse of the system.

2 Experimental setup

In this chapter we will present the experimental setup used, given a special section to the Nanodroplet generations, the doping process and the data acquisition system. A sub-chapter is also dedicate to the single shot correlation data acquisition system tested specifically to this Master‘s project. The apparatus we worked with is part of the the group of Molecule and Nanophysics at the University of Freiburg, Germany, and was calibrated and used for the experiments in [51] and [28].

In figure XXX an sketch of the apparatus is shown. From left to right; The source chamber where the ultra cold molecular beams are produced, the central chamber or "doping chamber" where the beam gas is doped via pick up process using a gas doping cell or a diffuse oven for alkaloids where gases or thermally vaporized solids and using as dopant, the last chamber or "detection chamber" combines a VMI - TOF detection system and a Langmuir taylor (LT) detector. To generate the nano plasmas the apparatus was Used in two different institutions, at the Max Plank Institute for Nuclear Physics in Heidelberg and the Extreme light institute (ELI) in Szeged, Hungary, because of the special laser systems can be provided in there.

The following sections describes the essential components of the apparatus, taking special attention to the new Triggering systems implemented to correlate the VMI and TOF signals in the last part of the project. The structure where compacted to a length of about 240 cm long, each chamber has attached its own turbo pumps with pre-vacuum pumps and are separated by valves and skimmers. On one hand, this enables to manipulate the vacuum in an independent way and control the targets in the "detection chamber", on the other hand a allows an optimum adaptation of the suction power of the pumps to the gas load of the individual chambers as wheel as to ventilate and open, without having to disturb the entire system.

2.1 Source chamber

The Source chamber consists of a 6-way CF vacuum chamber, with a 2-stage cryostat power a cold-head that can be cooled down to 9K, located in entrance of the chamber, parallel to the floor with an attached conical nozzle for the gas expansion process.

The cooling capacity of the cryostat consists of a copper tube, into which pre-cooled helium is introduced. It can be adjusted by operating two heating resistors in combination with a sensor diode for temperature measurement and a PID controller. Controlling the resistor current the temperature at the end of the nozze can be keeping it stable. The conical nozzle used to generate the atomic beam is the standard used in the research group on Nanoplasma reasearch directed by Prf, frank Steankeirmeyer at Freiburg University. It is made of copper and has a platinum plate on front with a hole of $5\mu m$ of diameter for He experiments and $15\mu m$ for Ne gas clusters. The diameters where choseen in order to follow the Size dependence of the *Hagenas* "law", which together with the adjustable gas pressure and the nozzle temperature regulates the flow. The cold head-nozzle arrangement are connected to the chamber via a self-made x-y manipulator, with a thermally insulating rubber? ring, which allows a beam adjustment in relation to the other components in the setup with out braking the vacuum. At the bottom of the chamber an "Agilent" turbo pump of $1800L/s$ capacity is attached to a pre-vacuum scroll pump as exhaust. A skimmer with a diameter of $400\mu m$ is located in front of the effusive jet, sorting the gas beam not just by it size but also by its velocity vectors and allowing just those beams with direction to the further vacuum chambers. To adjust the nozzle optimally to the skimmer,it is connected to an x-y displacement unit and can be aligned from outside the vacuum chamber. To prevent the small opening of the nozzle from clogging over time, high-purity helium 6.0 (99.9999% purity) and Ne 5.0 (99.999% purity) is used and can also be used outside of the measurements ensures a constant gas flow through the nozzle. At this extreme temperatures this prevents that any impurity in the gas bottle can condensate, blocking the nozzle or changing the conditions of the clusters production.

2.2 Dopping chamber

As explained in the chapter above, the Doping takes place by inelastic impacts with atoms from the gas phase, referenced as the pick-up thecnique. In this experiment we doped with both metals and noble gases, and two different methods of doping are used: Metals are heated in evaporated phase in a oven, while gas dopant yield in a Gas doping cell entered the vacuum chamber through a needle valve. on the next section we will explain the elements of the dopping cham,ber and its most important characteristics used.

The oven chamber is conected after to the Source chammber via the skimmer, it is also a 6-way CF vacuum chamber, with a turbo pump on bottom, connected

to it own pre-vacum scroll pump. On the sides the flanks allows a cold trap not used in this experiment, on the other side the flank that permit connection to the oven and the vacuum sensor. The Skimmer is made of Niquel??, a very thin metal easy to bend, so in order to prevent stronf pressures diferrence in the chamber that can modify the skimmer, a bypass is conected between the two chamber using a stainlees steel flexible hose. An internal stand is welded to the front of the chamber and aligned with the skimmer. This stand supports the Chopper, the gas dopping cell and the oven. In the front the rail the choppers is located. It is an steel disk with three notches uniformed located,two photocell around the bottom of the disk reads the position of the bottom notches so the upper one can be positioned right in front the skimmer. In this way, when the disk rotates the beam can pass or its block by the disk in a controlled way.

After the chopper, there is the Gas Dopping cell, a circular flat metal base with a self modified KF hose. The base makes the base cell have a matching patter so the hose can be easy put and remove with out losing the alignment. The stainless steel flexible hose has two $5mm$ hole (one in front and one opposite to it, some cm up the base) alligned to the skimmer so the gas bean can go thought. The hose is fix to the base and goes to the top of the chamber where it is connected to a "swaglog" niddle valve that allows to control the gas flux for doping the beam. A Pfiffer CMR375 Capacitive sensor is located after the niddle valve so a better control of the pressures, ans so of the number of dopants in the cluster can be achived. This bendable construction allows not just to remove the doping cell with out difficulty but also to fit it on the top with out depending on a fix way to located the top plank, in this way there is room for maniouver and the construction is faster.

Finally at the end of the rail lies the Oven. As shown in fig XXX the oven consist on a patterned base (similar to the gas cell) that can move a few mm on $x-y$ plane. Over it, a metal cylinder with 4 heating cartridges holds a movable crucible in the center that contains the dopant sample, this movable container is set down by a rod that comes from the top of chamber after a valve. Both, the stove and crucible have holes (a conical entrance of $40mm$ diameter and $3mm$ diameter respectively) that allows the pass of the gas beam and are aligned to the beam pad, in this way the passing Atomic beam takes dopants via collisions with vaporized sample material.

One important advantage of this new oven design done by *Dominic Schomas*, is that the dopant can be change with out braking the vacuum, it was test in this experiments and prove to be useful saving time and effort. To control the temperature of the oven a temp sensor is fix in the stove, and the resistors current is manage by a PID controller allowing a stable temperature during the experiment.

VMI	Repeler	Extractor	Lens
X1	-2430	-1940	3500
X3	-7290	5820	10500
Ion	2430	1940	0

The maximal temperature reached was $450°c$, enough to creates the gas phase for the potassium K and calcium Ca used in this experiment as shown in the table XXXX. Finally there is an extra skimmer of diameter XXX fixed to a valve between the connection of the doping chamber and the detection chamber that helps to avoid the disperse beams or an overflow from one chamber to the other.

In addition to the doped gas nano droplets, effusive gas is also released from the dopant chamber into the detector chambers through a "swarlog niidle valve" and can be ionized and detected there. This disperse gas was pour in directly on the chamber or filtered by diffusive atoms going out of the oven and passing across the second skimmer once the choppers is close. This atomic gases where added for calibration of the detectors and background reduction allowing just one gas at a time.

2.3 Detection chamber

As mentioned, the detector chamber is connected to the Oven chamber via a valve and a skimmer. The detector chamber contains a newly developed Velocity-Map-Imaging spectrometer on top, a time-of-flight mass spectrometer on bottom and a Lt detector on front. on this section we will give a brief presentation of the VMi and the TOf used in this experiment, but taking spacial detaile in the new Triggering process that allows us to get the single nanoplasma explotions that we are interest on.

2.3.1 Velocity map imaging VMI

The VMI detector used in this experiment is detail in [51], this construction basically follows the standard geometry of Eppink and Parker [14]. Its composed by three electro lenses (repeler, lens and extractor) that focuses the ions or electron on a $86,6mm$ (effective area) diameter Micro channel plates (MCP) arrange. This detector set is basically two MCPs overposed by 90 degrees each other and a phosphoscreen (PS) layer of same diameter facing the top of the chamber to a Ca-fluoride glass of $1mm$ thick, and a CCD camera focuced on the phosphorlayer.

The voltages applied to the MCP and PS determine the brightness of the final pictures of the ions, so in general just one set of voltages were use, around $1400V$

for the MCP and $4000V$ for the Ps. The achievable energy acceptance for this stack is $34eV$ for a the VMI setting 1 and $270eV$ for the X3 settings. The VMNI have a resolution of $\triangle E/E \leq 4\%$ [51]. The camara used in the experiment was a Basler acA1920-155um focused on the PS.

On fig **??** we present a view of the model of the VMI used in this experiment, From botom to top, the structure of the electrodes consists of two repeller electrodes separated by a few millimetres with circular openings on which a fine mesh copper grid is applied, an aperture electrode as extractor, another aperture electrode which is held at ground potential and then from the extended lens electrode with the following second ground electrode. At top the MCP-PS arrange (o black the MCP and on gray the PS) facing the center of the window instales in the top blanck of the chamber. Around thewwindow there are three conections that allows the voltages for the electrodes and the cables are carefully arrange around tthe structure to avoid discharges or even disturb the uniform electrical field.

The openings of the repeller (on bottom in bluish color) electrodes allow the use of these electrodes as well as extractor electrodes for a TOF spectrometer. In simultaneous operation of the VMI and the TOF spectrometer, the glued grids prevent mutual field effects of the two spectrometers. The repeller and extractor are grade 2 titanium and the lens is stainless.

2.4 Time of flight spectrometer

The TOF spectrometer used was designed by Wiley and McLaren [**?**]. As it names reefers, the TOF mass spectrometer relates the time that a particle on a electric field requires to reach certain distance with its mass, when atoms and molecules are photoionized, they pass through an electrostatic acceleration field and are registered in a detector after crossing a field-free flight path. On the basis of the flight duration the ratio m/q of a particle can be determined as:

$$t - t_0 = a\sqrt{\frac{m}{q}} \tag{2.1}$$

Where a is a experimental factor depending of the flight distance, electric fields and material of the setup, m/q is the relation mass - charge, t_0 is the time ionization time (given by the laser)and t is the time of flight.

The ions creation takes place between the planar repellers and extractor aperture electrodes. Behind the extractor electrode there is a further aperture electrode, which is held at zero potential and thus generates a further flight route with a defined

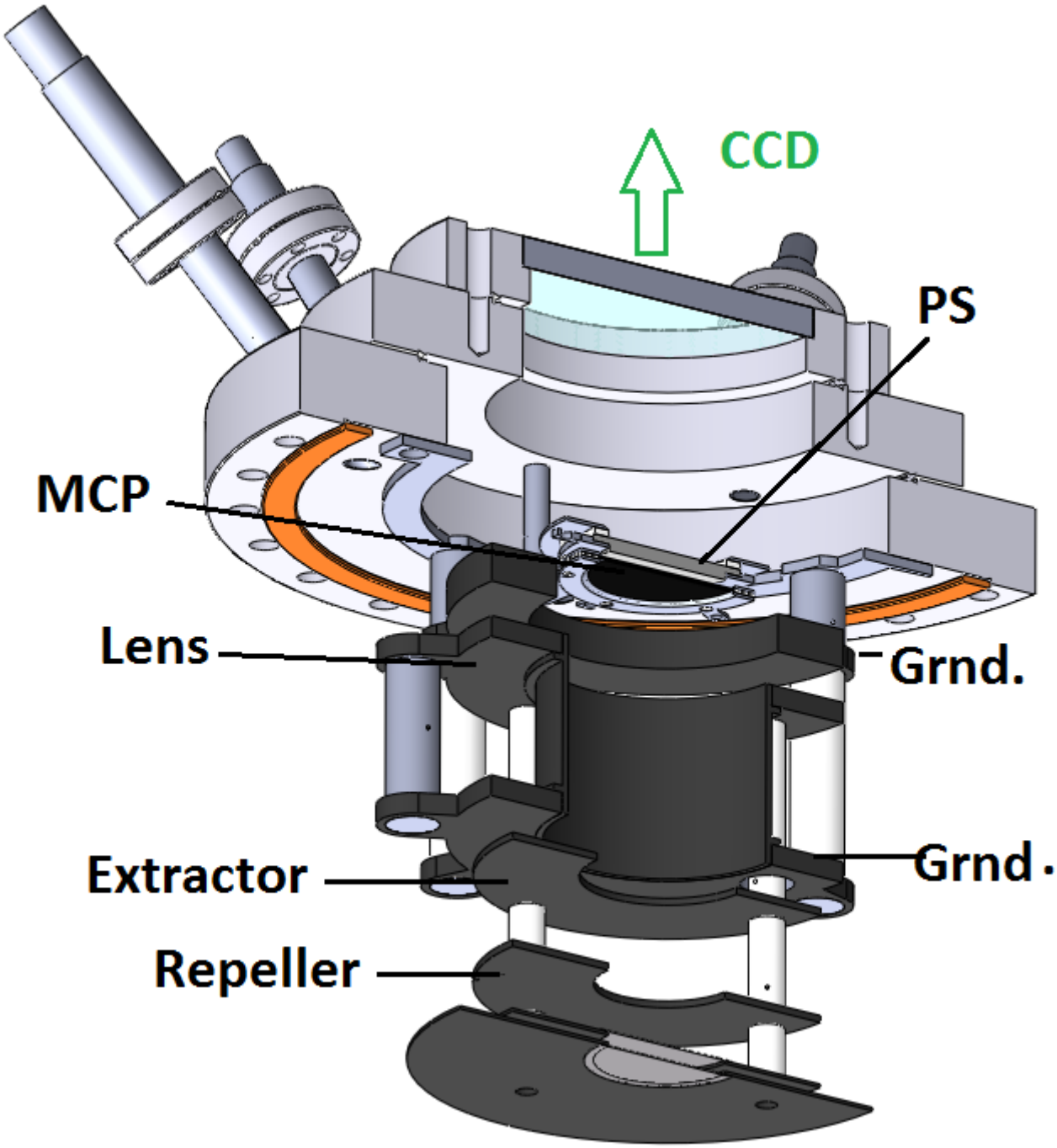

Figure 2.1: Sectional cut view of the CAD model of the spectrometer setup. On black are the are the electrodes and the white the Polyether ether ketone (PEEK) insolators. On ornange, the cooper ring ang on blue the top window facing the cCCD camera

field, Grids are glued to the openings of the electrodes to prevent the propagation of the fields through the orifices in the electrodes. The repeller electrode is set to a positive potential and the extractor to a negative potential. The resulting electric field accelerates the ions through the openings in the flight tube, on which grids are mounted on both sides to keep the drift path free of field. Onece the coulomb explotion takes places, the ions are accelerated by the electric field of the repeller and then fly through a field-free drift path to the detector. This allows a complete mass spectrum to be recorded within a few microseconds in a single measuring step [?].

The flying Ions finally are detected by a Daly detector [?]. It consists of a cup, a grid and a ring. The cup lies on negative High voltage while the ring on positive. The ions from the repeller pass trough the field free tube corrected by a drift electrosde. Since in the direction of the hole the potential for electrons drops sharply. The ring electrode generates an E-field, which directs the ions into the cup. The ions that pass the the grid at high speed hits on the bottom of the cup, they generate some electrons, which are transmitted through a small hole in the Cup and then in a scintillator Eljen thechnilogy(EJ-204) that flashes some photons in the process. These are detected in a Hammamatzu r-647 photomultiplier. The voltage output of the photomultiplier is controlled by a fast analog-to-digital converter, and its used at a $900V$ voltage. The cup and the drift-scintelator tube where set at high voltages, $-17000V$ and -4000 respectively.

2.5 Lt detector

The Langmuir-Taylor detector (LT detector) chamber consists of a small CF40-6-way chamber. The detector consists essentially of an annealing filament, which is located between two planar round electrodes. The Operating Principle of an LT-Detector is based on surface ionisation by the tunnel effect [?]. For the annealing filament is typically used for rhenium, platinum or tungsten, as this is the most common has a comparatively high electron work function. As a consequence, a passing neutral atoms is ionized by the heated wire, releasing an electron into the wire. The resulting ions is attracted by the negative electrodes around the wire generating a current. The ionic current generated at the electrodes is proportional to the number of ionized atoms and is measured using a picoampermeter. The LT chamber is connected to the VMI chamber via an orifice plate and is used mainly ad a beandump also as a alingment detector. The most current generated on the chamber the most atoms arte passing thourgtthe hole, so we can be sure that the beam pad is in the midle of the VMI repellers and extractor and the reaction takes

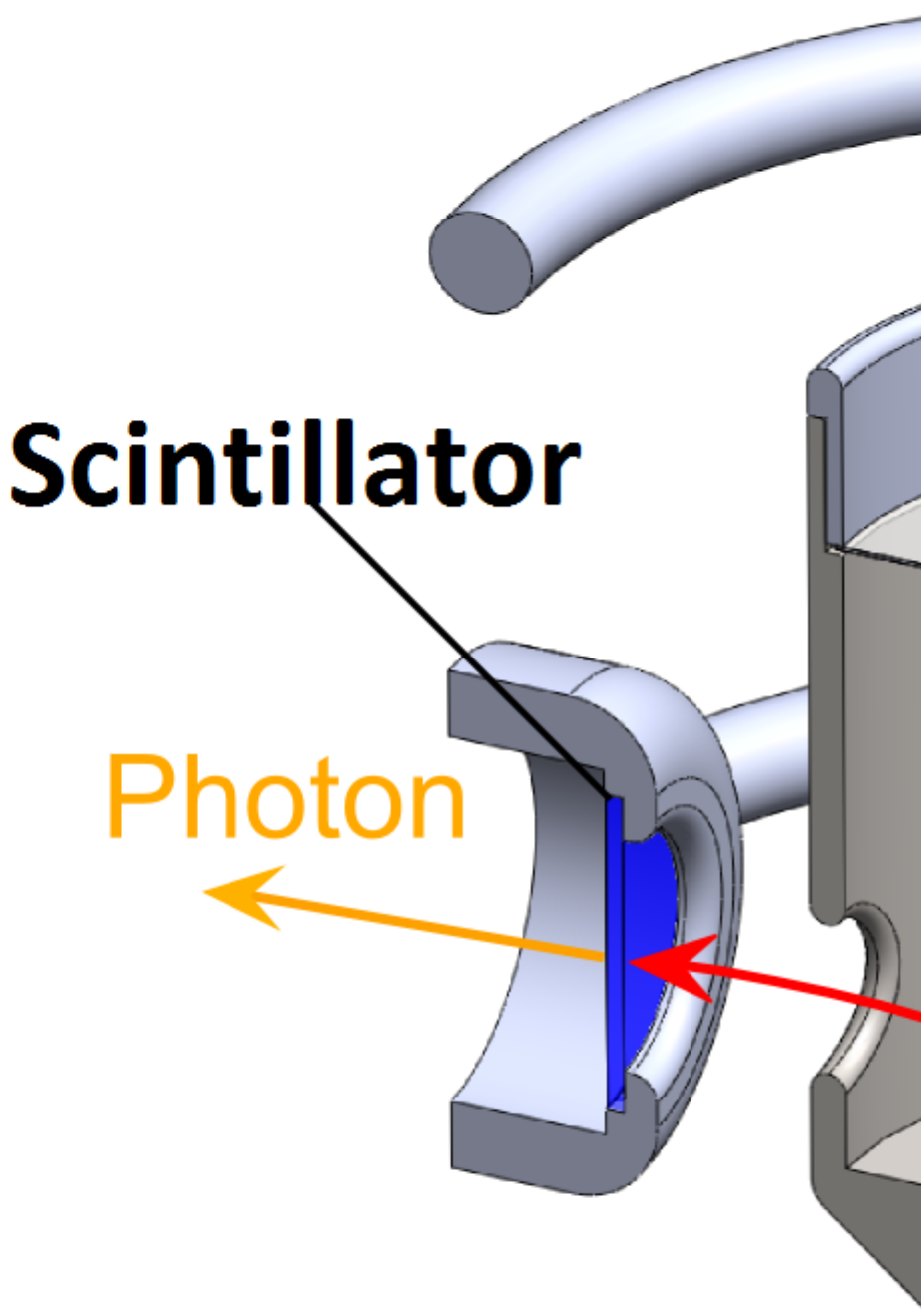
Scintillator
Photon

List delays

Channel	Set to:
A	$= T + 0$
B	$= T + 1\mu s$
C	$= BorB + 6\mu s$

places in the rigth area.

2.6 Camera and trigger protocol

The idea of this master thesis was to achive individual single shots nanoplasma explosion data in the camera (VMI) and TOF. The advantage of this correlation is the ability of threat the data in invidvidual ways, reduce the bacground in the images and achive possible properties in the coulomb explosion that are not possible when threated with averaged data.

in order to achive it, a first aproche was done doing a sofware triggering in the CCD camera software and the osciloscope for the TOF, an Acqiris Card CC103. The main idea was using LabView an external clock (a RasberryPi) was triggered by the laser, when the explosion should start, and at the same time it software trigger the camera and osciloscope programs to start the acquicition. Having all the data acquire in the same program would allow to sort the data online and reduce the storage needed to the experiment. The Labview program was tested unsusesfull for the data acquisition rate needed in ELI $100KHz$, the main problem where that using software triggering more delay are aplied due the operating system and the comunication protocols, so even the data where acquire at the same time the delays at saving the information in the hard drive made impossible to correlate the signals.

Based on this same idea, a second aprove was used. In replacement odf a software ttrigering a ghardware triggering was used. The main idea remained, the laser triggers a dely generator that at the same time triggers the osciloscope, a RS RTO2000 with bandwith of 600MHZ to 6GHz, and the camara. Two facts had to been taken into account. First, our camera cant go lower than $34\mu s$ in exposure time. Second, the timing between the camera reciving the trigger and starting the acqisition was n ot negligible as it was for thze osciloscope, as we measure, the camera took between $5 - 6\mu s$ to start after the trigger was send. To solve this problem thetriggering scheme in fig XXX was used.

A delay generator (Stanford Research Systems MD DG335) recive the laser trigger (100KHz) channel B and C where conected to the osciloscope to chanel 1 and 2 respectivelly, and chanel A was conected to the pin 1 (trigger) on the camera. Lets

remember that the due the minimal exposure time of the camera, we can not identify a single laser shot with it. Table ?? shows the deays used in the experiment, where T is the original laser trigger and A,B and C are the channels in the delay generator. In this way, it can be shown in fig, that the osciloscope can "see" each of the laser shots individually but the camera will see at least 3 shots, but fortunatelly, not each laser shot generates signal, as show in the next chapter in general just $10 to 20\%$ of the laser short ignites a plasma explosion, this mean that almos most of the pictures will have no signal, some of them can have one or more explosion, but the main of them will contain just one signal explosion in the vmi that in the data anaöisis can be correlated to its individual TOF signal.

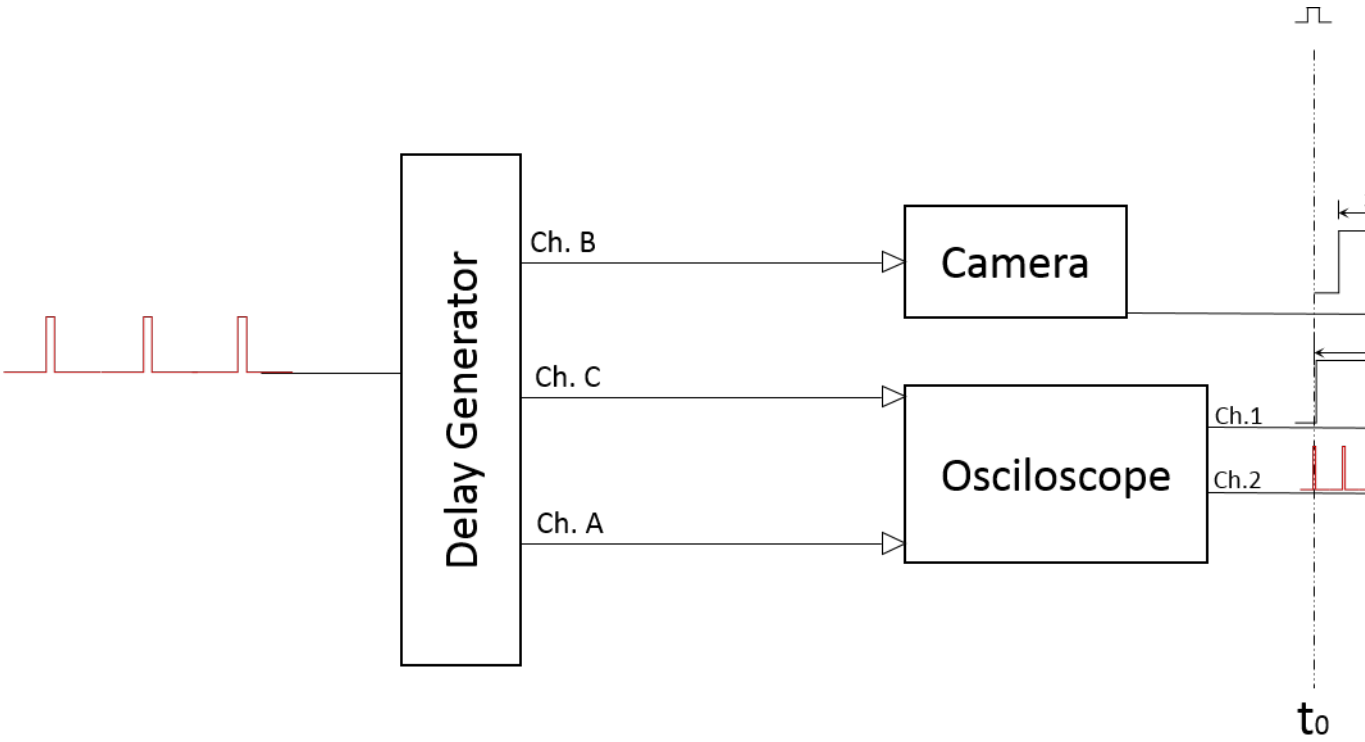

Figure 2.3: Schem of the trigger system used on

In Fig ??, we show the simplies Trigger scheme used in the experiment. The osciloscope and camera is trigered by the delayed channel B. The osciloscope is set to $50\mu s$ and the camarta to the minimal exposure time. So the camara and osciloscope sees the same trigger, the osciloscope will record at least 5 laser shots, but the camera because starts later just can see three as shown. The pictures are saved in the memory RAM of the computer so the dead time after the camara is off is mandatory to give the operative system enougth time to save the data on disk and dont full the Ram. A small improvement in this system can be done if we trigger the camara with B and the oscilloscope with C, so both apparatus can start almost at

the same time and no corrections needs to be done. Each of the data set are saved with a unique label that will help to correlate the data after. Once a explosion is found in the VMI pictures, we check in its corresponding TOF that it have just one signal in all five laser shots, so we can be sure that picture correspond to a single coulomb explosion, in case more than one signal is found, this picture is discard.

List of Figures

List of Tables

3 Bibliography

[1] *Helium*. http://ltl.tkk.fi/research/theory/helium.html

[2] Becker, U. (Hrsg.) ; Shirley, D. A. (Hrsg.): *VUV and Soft X-Ray Photoionization*. http://dx.doi.org/10.1007/978-1-4613-0315-2

[3] A. Bethe, H. ; E. Salpeter, E. : *The Quantum Mechanics of One- and Two-Electron Atoms*. Bd. 35. http://dx.doi.org/10.1007/978-3-662-12869-5. http://dx.doi.org/10.1007/978-3-662-12869-5

[4] Atkins, K. R.: *Liquid Helium*. Cambridge University Press. – ISBN 978–1–107–63890–7. – Google-Books-ID: gzmNAwAAQBAJ

[5] Berkowitz, J. : *Photoabsorption, photoionization, and photoelectron spectroscopy*. Academic Press. – ISBN 978–0–12–091650–4. – Google-Books-ID: POeHAAAAIAAJ

[6] Bünermann, O. ; Stienkemeier, F. : Modeling the formation of alkali clusters attached to helium nanodroplets and the abundance of high-spin states. 61, Nr. 3, 645–655. http://dx.doi.org/10.1140/epjd/e2011-10466-0. – DOI 10.1140/epjd/e2011–10466–0. – ISSN 1434–6079

[7] Buchenau, H. ; Knuth, E. L. ; Northby, J. ; Toennies, J. P. ; Winkler, C. : Mass spectra and time-of-flight distributions of helium cluster beams. 92, Nr. 11, 6875–6889. http://dx.doi.org/10.1063/1.458275. – DOI 10.1063/1.458275. – ISSN 0021–9606, 1089–7690

[8] Christen, W. ; Rademann, K. ; Even, U. : Supersonic Beams at High Particle Densities: Model Description beyond the Ideal Gas Approximation †. 114, Nr. 42, 11189–11201. http://dx.doi.org/10.1021/jp102855m. – DOI 10.1021/jp102855m. – ISSN 1089–5639, 1520–5215

[9] Connerade, J. P.: *Highly Excited Atoms*. Cambridge University Press. – ISBN 978–0–521–43232–0. – Google-Books-ID: VgpkXDfkqYEC

[10] Delft, D. van ; Kes, P. : The discovery of superconductivity. 63, Nr. 9, 38–43. http://dx.doi.org/10.1063/1.3490499. – DOI 10.1063/1.3490499. – ISSN 0031–9228

[11] Ditmire, T. ; Donnelly, T. ; Rubenchik, A. M. ; Falcone, R. W. ; Perry, M. D.: Interaction of intense laser pulses with atomic clusters. 53, Nr. 5, 3379–3402. http://dx.doi.org/10.1103/PhysRevA.53.3379. – DOI 10.1103/PhysRevA.53.3379

[12] Einstein, A. : Über einen die Erzeugung und Verwandlung des Lichtes betreffenden heuristischen Gesichtspunkt. 322, Nr. 6, 132–148. http://dx.doi.org/10.1002/andp.19053220607. – DOI 10.1002/andp.19053220607. – ISSN 1521–3889

[13] Enss, C. ; Hunklinger, S. : *Low-Temperature Physics*. Springer-Verlag //www.springer.com/de/book/9783540231646. – ISBN 978–3–540–23164–6

[14] Eppink, A. T. J. B. ; Parker, D. H.: Velocity map imaging of ions and electrons using electrostatic lenses: Application in photoelectron and photofragment ion imaging of molecular oxygen. 68, Nr. 9, 3477–3484. http://dx.doi.org/10.1063/1.1148310. – DOI 10.1063/1.1148310. – ISSN 0034–6748

[15] Erk, B. : *Nobel cluster gas expansion driven by a ultra-short high intensity infrared laser*

[16] Fennel, T. ; Meiwes-Broer, K.-H. ; Tiggesbäumker, J. ; Reinhard, P.-G. ; Dinh, P. M. ; Suraud, E. : Laser-driven nonlinear cluster dynamics. 82, Nr. 2, 1793–1842. http://dx.doi.org/10.1103/RevModPhys.82.1793. – DOI 10.1103/RevModPhys.82.1793

[17] Fermi, E. : Quantum Theory of Radiation. 4, Nr. 1, 87–132. http://dx.doi.org/10.1103/RevModPhys.4.87. – DOI 10.1103/RevModPhys.4.87

[18] Gaveau, M.-A. ; Briant, M. ; Vallet, V. ; M. Mestdagh, J. ; P. Visticot, J. : Reaction Between Barium and N2O on Large Neon Clusters. http://dx.doi.org/10.1007/978-3-642-56800-8_57. – DOI 10.1007/978–3–642–56800–$8_5$7. – $-ISBN978--3--642--63150--4, S.827--838$

[19] Gough, T. E. ; Mengel, M. ; Rowntree, P. A. ; Scoles, G. : Infrared spectroscopy at the surface of clusters: SF6 on Ar. 83, Nr. 10, 4958–4961.

http://dx.doi.org/10.1063/1.449757. – DOI 10.1063/1.449757. – ISSN 0021–9606

[20] Grebenev, S. ; Toennies, J. P. ; Vilesov, A. F.: Superfluidity Within a Small Helium-4 Cluster: The Microscopic Andronikashvili Experiment. 279, Nr. 5359, 2083–2086. http://dx.doi.org/10.1126/science.279.5359.2083. – DOI 10.1126/science.279.5359.2083. – ISSN 0036–8075, 1095–9203

[21] Griffiths, D. J.: *Introduction to electrodynamics*. Fourth edition. Pearson. – ISBN 978–0–321–85656–2

[22] Grüner, B. : *Femtosekundenspektroskopie an dotierten Heliumnanotröpfchen: Dissipative Vibrationsdynamik und Charakterisierung eines Nanoplasmas*

[23] Hagena, O. F. ; Obert, W. : Cluster Formation in Expanding Supersonic Jets: Effect of Pressure, Temperature, Nozzle Size, and Test Gas. 56, Nr. 5, 1793–1802. http://dx.doi.org/10.1063/1.1677455. – DOI 10.1063/1.1677455. – ISSN 0021–9606

[24] Hagena, O. F. ; Obert, W. : Cluster Formation in Expanding Supersonic Jets: Effect of Pressure, Temperature, Nozzle Size, and Test Gas. 56, Nr. 5, 1793–1802. http://dx.doi.org/10.1063/1.1677455. – DOI 10.1063/1.1677455. – ISSN 0021–9606

[25] Halperin, W. P. ; Rasmussen, F. B. ; Archie, C. N. ; Richardson, R. C.: Properties of melting 3He: Specific heat, entropy, latent heat, and temperature. 31, Nr. 5, 617–698. http://dx.doi.org/10.1007/BF00116046. – DOI 10.1007/BF00116046. – ISSN 1573–7357

[26] Harms, J. ; Toennies, J. P. ; Dalfovo, F. : Density of superfluid helium droplets. 58, Nr. 6, 3341–3350. http://dx.doi.org/10.1103/PhysRevB.58.3341. – DOI 10.1103/PhysRevB.58.3341

[27] Haught, A. F. ; Polk, D. H.: Formation and Heating of Laser Irradiated Solid Particle Plasmas. 13, Nr. 11, 2825–2841. http://dx.doi.org/10.1063/1.1692869. – DOI 10.1063/1.1692869. – ISSN 0031–9171

[28] Heidenreich, A. ; Grüner, B. ; Schomas, D. ; Stienkemeier, F. ; Krishnan, S. R. ; Mudrich, M. : Charging dynamics of dopants in helium nanoplasmas. http://dx.doi.org/10.1080/09500340.2017.1281454. – DOI 10.1080/09500340.2017.1281454

[29] Kamenev, A. : Introduction to the Keldysh Formalism.

[30] Kapitza, P. : Viscosity of Liquid Helium below the -Point. 141, Nr. 3558, 74. http://dx.doi.org/10.1038/141074a0. – DOI 10.1038/141074a0. – ISSN 1476–4687

[31] Karnakov, B. M. ; Mur, V. D. ; Popruzhenko, S. V. ; Popov, V. S.: Strong field ionization by ultrashort laser pulses: Application of the Keldysh theory. 374, Nr. 2, 386–390. http://dx.doi.org/10.1016/j.physleta.2009.10.058. – DOI 10.1016/j.physleta.2009.10.058. – ISSN 0375–9601

[32] KELDYSH, L. V.: Ionization in the field of a strong electromagnetic wave. 20, 1307. https://ci.nii.ac.jp/naid/10006486551/

[33] Knuth, E. L. ; Henne, U. : Average size and size distribution of large droplets produced in a free-jet expansion of a liquid. 110, Nr. 5, 2664–2668. http://dx.doi.org/10.1063/1.477988. – DOI 10.1063/1.477988. – ISSN 0021–9606, 1089–7690

[34] Krishnan, S. R. ; Fechner, L. ; Kremer, M. ; Sharma, V. ; Fischer, B. ; Camus, N. ; Jha, J. ; Krishnamurthy, M. ; Pfeifer, T. ; Moshammer, R. ; Ullrich, J. ; Stienkemeier, F. ; Mudrich, M. : Ignition of Doped Helium Nanodroplets in Intense Few-Cycle Laser Pulses. In: Yamanouchi, K. (Hrsg.) ; Katsumi, M. (Hrsg.): *Multiphoton Processes and Attosecond Physics*, Springer Berlin Heidelberg (Springer Proceedings in Physics). – ISBN 978–3–642–28948–4, S. 385–390

[35] Krishnan, S. R.: Doped helium nanodroplets in intense few-cycle infrared pulses. http://inis.iaea.org/Search/search.aspx?orig_q=RN:43095633

[36] Last, I. ; Jortner, J. : Quasiresonance ionization of large multicharged clusters in a strong laser field. 60, Nr. 3, 2215–2221. http://dx.doi.org/10.1103/PhysRevA.60.2215. – DOI 10.1103/PhysRevA.60.2215

[37] Lewerenz, M. ; Schilling, B. ; Toennies, J. P.: Successive capture and coagulation of atoms and molecules to small clusters in large liquid helium clusters. 102, Nr. 20, 8191–8207. http://dx.doi.org/10.1063/1.469231. – DOI 10.1063/1.469231. – ISSN 0021–9606

[38] Lewis, W. K. ; Harruff-Miller, B. A. ; Leatherman, P. ; Gord, M. A. ; Bunker, C. E.: Helium droplet calorimetry of strongly bound species: Carbon clusters from C $_2$ to C $_{12}$. 85, Nr. 9, 094102. http://dx.doi.org/10.1063/1.4895670. – DOI 10.1063/1.4895670. – ISSN 0034–6748, 1089–7623

[39] Madison, K. W. ; Patel, P. K. ; Allen, M. ; Price, D. ; Fitzpatrick, R. ; Ditmire, T. : Role of laser-pulse duration in the neutron yield of deuterium cluster targets. 70, Nr. 5. http://dx.doi.org/10.1103/PhysRevA.70.053201. – DOI 10.1103/PhysRevA.70.053201. – ISSN 1050–2947, 1094–1622

[40] Mainfray, G. : MULTIPHOTON IONIZATION OF ATOMS.

[41] Meija, J. ; Coplen, T. B. ; Berglund, M. ; Brand, W. A. ; De, B. P. ; Gröning, M. ; Holden, N. E. ; Irrgeher, J. ; Loss, R. D. ; Walczyk, T. ; Prohaska, T. : Atomic weights of the elements 2013 (IUPAC Technical Report). 88, Nr. 3, 265–291. http://dx.doi.org/10.1515/pac-2015-0305. – DOI 10.1515/pac–2015–0305. – ISSN 0033–4545

[42] Mikaberidze, A. : *Atomic and molecular clusters in intense laser pulses.* https://www.pks.mpg.de/mpi-doc/rostgruppe/dissertation/mikaberidze_dissertation.pdf

[43] Nauta, K. ; Miller, R. E.: Nonequilibrium Self-Assembly of Long Chains of Polar Molecules in Superfluid Helium. 283, Nr. 5409, 1895–1897. http://dx.doi.org/10.1126/science.283.5409.1895. – DOI 10.1126/science.283.5409.1895. – ISSN 0036–8075, 1095–9203

[44] Pietrowski, R. von ; Rutzen, M. ; Haeften, K. von ; Kakar, S. ; Möller, T. : Fluorescence excitation spectroscopy of Xenon doped Neon clusters: Size and site effects, and cluster melting. 40, S. 22–24. http://dx.doi.org/10.1007/s004600050149. – DOI 10.1007/s004600050149

[45] Popruzhenko, S. V.: Keldysh theory of strong field ionization: history, applications, difficulties and perspectives. 47, Nr. 20, 204001. http://dx.doi.org/10.1088/0953-4075/47/20/204001. – DOI 10.1088/0953–4075/47/20/204001. – ISSN 0953–4075

[46] Protopapas, M. ; Keitel, C. H. ; Knight, P. L.: Atomic physics with super-high intensity lasers. 60, Nr. 4, 389–486. http://dx.doi.org/10.1088/0034-4885/60/4/001. – DOI 10.1088/0034–4885/60/4/001. – ISSN 0034–4885, 1361–6633

[47] Rafipoor, A. J. M.: *Two-Color Photoionization Experiments with Ultrashort Light Pulses on Small Atomic Systems*

[48] Rhodes, C. K.: Multiphoton Ionization of Atoms. 229, Nr. 4720, 1345–1351. http://dx.doi.org/10.1126/science.229.4720.1345. – DOI 10.1126/science.229.4720.1345. – ISSN 0036–8075, 1095–9203

[49] Saalmann, U. ; Siedschlag, C. ; Rost, J. M.: Mechanisms of cluster ionization in strong laser pulses. 39, Nr. 4, R39–R77. http://dx.doi.org/10.1088/0953-4075/39/4/R01. – DOI 10.1088/0953–4075/39/4/R01. – ISSN 0953–4075, 1361–6455

[50] Schmidt, V. : *Electron Spectrometry of Atoms using Synchrotron Radiation*. Cambridge University Press. – ISBN 978–0–521–55053–6

[51] Schomas, D. ; Rendler, N. ; Krull, J. ; Richter, R. ; Mudrich, M. : A compact design for velocity-map imaging of energetic electrons and ions. 147, Nr. 1. http://dx.doi.org/10.1063/1.4984076. – DOI 10.1063/1.4984076. – ISSN 0021–9606

[52] Stebbings, S. L. ; Süssmann, F. ; Yang, Y.-Y. ; Scrinzi, A. ; Durach, M. ; Rusina, A. ; Stockman, M. I. ; Kling, M. F.: Generation of isolated attosecond extreme ultraviolet pulses employing nanoplasmonic field enhancement: optimization of coupled ellipsoids. 13, Nr. 7, 073010. http://dx.doi.org/10.1088/1367-2630/13/7/073010. – DOI 10.1088/1367–2630/13/7/073010. – ISSN 1367–2630

[53] Stienkemeier, F. ; Lehmann, K. K.: Spectroscopy and dynamics in helium nanodroplets. 39, Nr. 8, R127–R166. http://dx.doi.org/10.1088/0953-4075/39/8/R01. – DOI 10.1088/0953–4075/39/8/R01. – ISSN 0953–4075, 1361–6455

[54] Stringari, S. ; Treiner, J. : Systematics of liquid helium clusters. 87, Nr. 8, 5021–5027. http://dx.doi.org/10.1063/1.452818. – DOI 10.1063/1.452818. – ISSN 0021–9606

[55] Swenson, C. A.: The Liquid-Solid Transformation in Helium near Absolute Zero. 79, Nr. 4, 626–631. http://dx.doi.org/10.1103/PhysRev.79.626. – DOI 10.1103/PhysRev.79.626

[56] Tchaplyguine, M. ; Lundwall, M. ; Gisselbrecht, M. ; Öhrwall, G. ; Feifel, R. ; Sorensen, S. ; Svensson, S. ; Mårtensson, N. ; Björneholm, O. : Variable surface composition and radial interface formation in self-assembled free, mixed ArXe clusters. 69, Nr. 3, 031201. http://dx.doi.org/10.1103/PhysRevA.69.031201. – DOI 10.1103/PhysRevA.69.031201

[57] Toennies, J. P. ; Vilesov, A. F.: Spectroscopy of Atoms and Molecules in Liquid Helium. 49, Nr. 1, 1–41. http://dx.doi.org/10.1146/annurev.physchem.49.1.1. – DOI 10.1146/annurev.physchem.49.1.1

[58] Toennies, J. P. ; Vilesov, A. F.: Superfluid Helium Droplets: A Uniquely Cold Nanomatrix for Molecules and Molecular Complexes. 43, Nr. 20, 2622–2648. http://dx.doi.org/10.1002/anie.200300611. – DOI 10.1002/anie.200300611. – ISSN 1521–3773

[59] Wabnitz, H. ; Bittner, L. ; Castro, A. R. B. ; Döhrmann, R. ; Gürtler, P. ; Laarmann, T. ; Laasch, W. ; Schulz, J. ; Swiderski, A. ; Haeften, K. von ; Möller, T. ; Faatz, B. ; Fateev, A. ; Feldhaus, J. ; Gerth, C. ; Hahn, U. ; Saldin, E. ; Schneidmiller, E. ; Sytchev, K. ; Tiedtke, K. ; Treusch, R. ; Yurkov, M. : Multiple ionization of atom clusters by intense soft X-rays from a free-electron laser. 420, Nr. 6915, 482–485. http://dx.doi.org/10.1038/nature01197. – DOI 10.1038/nature01197. – ISSN 1476–4687

[60] Weinberger, P. : The discovery of thermodynamics. 93, Nr. 20, 2576–2612. http://dx.doi.org/10.1080/14786435.2013.784402. – DOI 10.1080/14786435.2013.784402. – ISSN 1478–6435

[61] Whittle, E. ; Dows, D. A. ; Pimentel, G. C.: Matrix Isolation Method for the Experimental Study of Unstable Species. 22, Nr. 11, 1943–1943. http://dx.doi.org/10.1063/1.1739957. – DOI 10.1063/1.1739957. – ISSN 0021–9606, 1089–7690

[62] Young, D. A.: PHASE DIAGRAMS OF THE ELEMENTS.

[63] Zhao, K. ; Zhang, Q. ; Chini, M. ; Wu, Y. ; Wang, X. ; Chang, Z. : Tailoring a 67 attosecond pulse through advantageous phase-mismatch. 37, Nr. 18, 3891–3893. http://dx.doi.org/10.1364/OL.37.003891. – DOI 10.1364/OL.37.003891. – ISSN 1539–4794

Danksagung

An dieser Stelle Danke

Erklärung

Hiermit versichere ich, die e ingereichte Arbeit selbständig verfasst und keine anderen als die von mir angegebenen Quellen und Hilfsmittel benutzt zu haben. Wörtlich oder inhaltlich verwendete Quellen wurden entsprechend den anerkannten Regeln wissenschaftlichen Arbeitens (lege artis) zitiert. Ich erkläre weiterhin, dass die vorliegende Arbeit noch nicht anderweitig eingereicht wurde.

Ort, Datum ..... Unterschrift .....